Letter | Editors' Suggestion

Magnon spectrum of altermagnets beyond linear spin wave theory: Magnon-magnon interactions via time-dependent matrix product states versus atomistic spin dynamics

Federico Garcia-Gaitan, Ali Kefayati, John Q. Xiao, and Branislav K. Nikolić*
Department of Physics and Astronomy, University of Delaware, Newark, Delaware 19716, USA

(Received 15 March 2024; revised 24 December 2024; accepted 2 January 2025; published 15 January 2025)

The energy-momentum dispersion of magnons, as collective low-energy excitations of a magnetic material, is routinely computed from an effective quantum spin Hamiltonian but simplified via linearized Holstein-Primakoff transformations to describe noninteracting magnons. The dispersion produced by such linear spin wave theory (LSWT) is then plotted as "sharp bands" of infinitely long-lived quasiparticles. However, magnons are prone to many-body interactions with other quasiparticles—such as electrons, phonons, and other magnons—which can lead to shifting (i.e., band renormalization) and broadening of the sharp bands as a signature of a finite quasiparticle lifetime. The magnon-magnon interactions can be particularly important in antiferromagnets, and, therefore, possibly in newly classified altermagnets sharing many features of collinear antiferromagnets. Here, we employ nonperturbative quantum many-body calculations via time-dependent matrix product states (TDMPSs) to obtain the magnon spectral function for a RuO_2 altermagnet whose effective quantum spin Hamiltonian is put onto a four-leg cylinder. Its upper band is shifted away from the upper sharp band of LSWT, as well as broadened, which is explained as the consequence of *hybridization* of the latter with the three-magnon continuum. This implies that two-magnon Raman scattering spectra *cannot* be computed from LSWT bands, which offers a litmus test for the relevance of magnon-magnon interactions. Finally, we employ atomistic spin dynamics (ASD) simulations based on the classical Landau-Lifshitz-Gilbert (LLG) equation to obtain the magnon spectrum at finite temperature and/or at a fraction of the cost of TDMPS calculations. Despite including magnon-magnon interactions via the nonlinearity of the LLG equation, ASD simulations *cannot* match the TDMPS-computed magnon spectrum, thereby signaling *nonclassical* effects harbored by antiferromagnets and altermagnets.

DOI: 10.1103/PhysRevB.111.L020407

Introduction. Energy-momentum dispersion, routinely displayed [1] as "sharp bands" along high-symmetry paths in the Brillouin zone, is a fundamental property of quasiparticle collective excitations in solids, such as electrons (in the sense of Landau quasielectrons), phonons, and magnons [1]. For example, diagonalization of a single-particle electron Hamiltonian, such as tight-binding [2] and first-principles [3] ones obtained from density functional theory (DFT), yields bands whose sharpness signifies infinitely long-lived quasielectrons [1]. However, in the presence of Coulomb interaction effects that are beyond mean-field single-particle approaches [4], one has to resort to many-body calculations in which quasielectrons decay and their bands broaden to quantify their inverse lifetime [4,5]. Furthermore, when quasielectrons lose their identity completely, one obtains a continuum of energies of the so-called Hubbard bands [4,5].

An analogous situation exists in the case of magnons—quasiparticles introduced by Bloch [6] as a wavelike disturbance in the local magnetic ordering of a magnetic material. Their quanta [7] of frequency ω behave as bosonic quasiparticles carrying energy $\hbar\omega$, spin $\hbar$, and quasimomentum $\hbar\mathbf{q}$. The sharp bands, $\hbar\omega$ vs $\mathbf{q}$ (as exemplified by red and orange lines in Fig. 1), are routinely computed by extracting parameters of effective spin Hamiltonians [12] from DFT [11], which is then fed into Holstein-Primakoff (HP) [13] transformations that map original spin operators to bosonic ones. By linearizing HP transformations [7,14], one obtains a Hamiltonian quadratic in bosonic operators which is, therefore, exactly diagonalizable and provides the foundation of the so-called linear spin wave theory (LSWT) [15–17]. However, experiments often measure [18–21] magnon damping, which is a problem of great interest for both basic research [15] and applications in magnonics [22,23]. The origin of magnon damping can be traced to magnon-magnon interactions, as described by second-quantized Hamiltonians containing products of three or more bosonic operators [7,15]; magnon-phonon interactions [20], especially relevant for recently discovered two-dimensional magnetic materials [19]; and magnon-electron interactions in magnetic metals [24–28] or in heterostructures involving metallic layers [29,30]. For example, the so-called Landau damping of magnons due to hybridization with the continuum of electronic Stoner excitations, where a single-electron spin flips while transitioning from an occupied state with a given spin projection to an empty state with an opposite spin projection, has been quantified using either random phase approximation applied to model Hamiltonians [31] or first-principles methods like time-dependent DFT [24,25]. Furthermore, magnon-magnon interactions can cause [15,17,32] magnon spontaneous decay,

*Contact author: bnikolic@udel.edu

 ©2025 American Physical Society

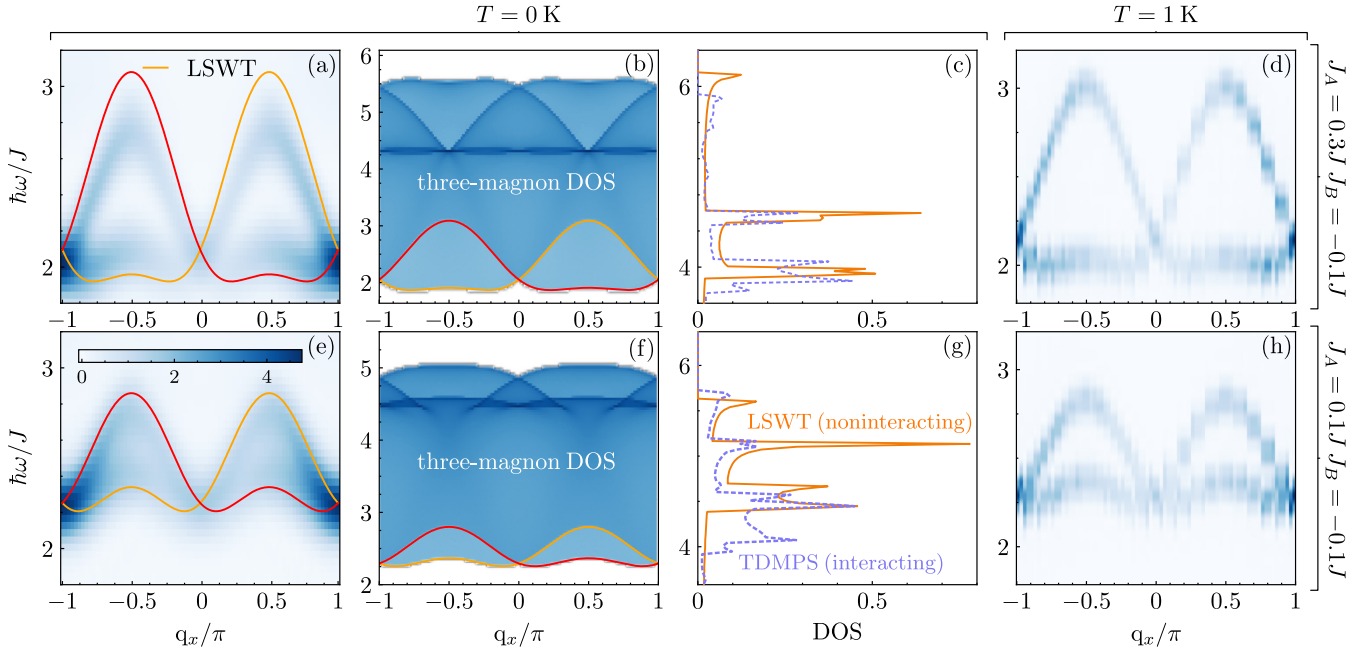

FIG. 1. (a) and (e) Magnon $\hbar\omega$ vs q_x spectrum of the RuO_2 altermagnetic spin Hamiltonian [Eq. (3)] for $q_y = \pi/2$ put onto the four-leg cylinder in Fig. 2. The dispersion is obtained either from the spectral function (blue trace) $A(q_x, \omega)$ [Eq. (2)], as computed from quantum many-body calculations via TDMPSs, or as sharp bands [red and orange lines plotting Eq. (5)] computed from one-body calculations via LSWT. (b) and (f) density of states (DOS) of the three-magnon continuum based [36] on one-magnon sharp bands in (a) and (e), respectively, plotted together with those sharp bands in order to examine whether one-magnon modes are energetically degenerate with the multimagnon continuum [36]. (c) and (g) One-magnon DOS for LSWT vs TDMPS bands, using doubled energy scales to allow for comparison [8] with experimental two-magnon RS spectra. (d) and (h) The same information as in (a) and (e), but obtained from classical ASD [9,10] simulations of DSSF $\mathcal{S}^{zz}(q_x, \omega)$ [Eq. (7)] at $T = 1$ K. The difference between the top and bottom rows is that in the top row we use exchange interactions $J_A \neq J_B$ between quantum spins localized at NN lattice sites obtained from DFT calculations in Ref. [11], while in the bottom row we artificially make them identical in absolute value. The color bar in (e) specifies values along blue traces in (a), (b), (d)–(f), and (h).

which broadens the sharp bands of LSWT; magnon band renormalization shifting them; and a renormalization of one-magnon wave functions as hybrids of different LSWT band eigenstates. Such effects are often encountered in insulating antiferromagnets [15,21,33], particularly noncollinear ones [32] or those hosting spin-orbit (SO) coupling effects [34], even down to zero temperature [34]; magnon topological insulators [17]; quantum paramagnets [28]; and quantum spin liquids [35,36].

Within quantum many-body theory, interaction-induced shifting/renormalization of magnon energies $\hbar\omega(\mathbf{q})$ and decay-induced lifetime (i.e., broadening of sharp bands) can be rigorously defined using a one-particle retarded Green's function (GF) [7,15,17,32],

$$G^{-1}(\mathbf{q}, \omega) = \hbar\omega - \hbar\omega(\mathbf{q}) - \Sigma(\mathbf{q}, \omega), \tag{1}$$

where $\Sigma(\mathbf{q}, \omega)$ is the self-energy due to interactions. Its real part renormalizes $\hbar\omega(\mathbf{q})$, while its imaginary part is responsible for the finite lifetime [15,17,32]. The self-energy can be computed *perturbatively* by evaluating selected Feynman diagrams containing loops [15,17,32]. Alternatively, one can compute the exact GF in Eq. (1) for spin Hamiltonians defined on low-dimensional lattices *nonperturbatively* via numerically exact diagonalization [7] or (quasi)exact algorithms based on time-dependent matrix product states (TDMPSs) [37]. These include [38] the original time-dependent density matrix renormalization group (tDMRG) [39–42] and time-dependent variational principle (TDVP) [43,44]. Instead of sharp bands of noninteracting magnons, one then plots (as we do in Fig. 1, obtained from TDMPSs) either the spectral function [7,15,32]

$$A(\mathbf{q}, \omega) = -\frac{1}{\pi}\mathrm{Im}\, G(\mathbf{q}, \omega), \tag{2}$$

or the dynamical spin structure factor (DSSF) $S(\mathbf{q}, \omega)$. The latter is directly measurable in neutron scattering experiments [21]. The quantities $A(\mathbf{q}, \omega)$ and $S(\mathbf{q}, \omega)$ can also be related to each other [45].

In particular, very recent analyses [16] revealed that LSWT producing sharp bands of noninteracting magnons can also introduce spurious symmetries, thereby leading to a magnon spectrum that can be far away from the correct one obtained from quantum many-body calculations via tDMRG [16]. One reason for this discrepancy arises when the Heisenberg effective spin Hamiltonian contains further than nearest-neighbor (NN) exchange interactions and they are not equal to each other. Another one is when antiferromagnets contain very different exchange interactions [16] within two sublattices. This is precisely the situation (top row of Fig. 1) encountered in RuO_2 as an early prototypical [46] example of altermagnetic material [47,48]. These newly established classes of magnets were originally considered [49–52] to be just another type of collinear antiferromagnets. They have attracted considerable attention due to their unusual fundamental properties

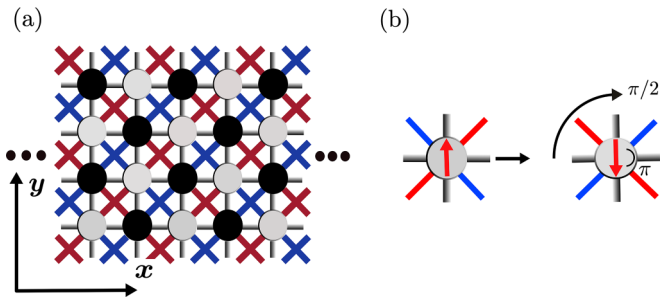

FIG. 2. (a) Quasi-one-dimensional lattice, shown as a four-leg cylinder because of the periodic boundary conditions imposed along the transverse y direction, onto which the effective spin Hamiltonian [Eq. (3)] of RuO_2 [11] is placed for TDMPS calculations. Its three different Heisenberg exchange interactions are depicted using three different colors: red and blue for intrasublattice interactions and gray for intersublattice interactions. (b) Illustration of the symmetry group connecting two sites (by $\pi/2$ rotation) or two spins (by π rotation) within the two sublattices in (a).

and potential applications in spintronics. Akin to ferromagnets, they exhibit time-reversal symmetry breaking and transport properties like the anomalous Hall effect, tunneling magnetoresistance, and magneto-optics [47,48]. This is due to antiferromagnetic ordering-induced momentum-dependent spin splitting of electronic bands, analogous to materials with SO-split electronic bands but without requiring noncentrosymmetric crystals and high atomic number elements underlying materials with large SO coupling [50]. The sharp bands of noninteracting magnons in RuO_2 have already been computed [11], exhibiting chirality akin to ferromagnets but with linear energy-momentum dispersion akin to antiferromagnets. The Landau damping [24,25,31] of magnons in RuO_2 was predicted in Ref. [11] to be suppressed by the spin-split electronic structure of altermagnets, but subsequent studies [53] found it to be finite and highly anisotropic with the ability to completely suppress magnon propagation along selected spatial directions. On the other hand, possible damping due to magnon-magnon interactions remains unexplored.

In this Letter, we compute the magnon spectrum of an altermagnetic spin Hamiltonian [11] of RuO_2 via three different methods. For reference, we first obtain chiral sharp bands of noninteracting magnons on the four-leg cylinder in Fig. 2 using LSWT [14,16]. Our LSWT also reproduces chiral bands of RuO_2 on the three-dimensional (3D) lattice from Ref. [11] (see the Supplemental Material (SM) [54]). For the same quasi-one-dimensional four-leg cylinder, we then compute the magnon spectrum encoded by $A(q_x, \omega)$ [Eq. (2)] as obtained via nonperturbative quantum many-body calculations based on a TDVP-implemented algorithm [39] for a magnonic retarded GF [Eq. (6)]. Finally, we extract the magnon spectrum from classical atomistic spin dynamics (ASD) [9,10,55] by calculating [9,10] the DSSF [Eq. (7)] from stochastic Landau-Lifshitz-Gilbert (LLG) equation based simulations of the same four-leg cylinder but hosting a classical spin vector on each site. The ASD simulations can take into account both magnon-magnon interactions [56] (as the LLG equation is nonlinear) and finite temperature (via noise terms in the LLG equation [55], but only at the *classical* level). Our principal results for quantum mechanically treated noninteracting [red and orange lines in Figs. 1(a) and 1(e)] and interacting [blue traces in Figs. 1(a) and 1(e)] magnons are shown in Fig. 1. In addition, the classical treatment of interacting altermagnetic magnons via ASD is shown in Figs. 1(d) and 1(h). Prior to discussing these results, we introduce useful concepts and notation.

Models and methods. We employ a Heisenberg Hamiltonian [11,12],

$$\hat{H} = J \sum_{\langle ij \rangle} \hat{\mathbf{S}}_i \cdot \hat{\mathbf{S}}_j + \sum_{\langle\langle ij \rangle\rangle} J_{ij} \hat{\mathbf{S}}_i \cdot \hat{\mathbf{S}}_j, \tag{3}$$

on a four-leg cylinder with periodic boundary conditions in the transverse direction (Fig. 2). Here, $\hat{\mathbf{S}}_i$ is the operator of $S = 1/2$ spin localized at site i of the lattice; $\langle ij \rangle$ denotes the summation over NN sites, and $\langle\langle ij \rangle\rangle$ denotes the summation over next-NN sites. Note that the exchange coupling J_{ij} is direction dependent and takes only two possible values, J_A and J_B, thereby taking into account altermagnetic electronic spectrum effects on the effective spin Hamiltonian. The specific values of the exchange interactions that we use, $J_A = 1.25$ meV and $J_B = -0.6$ meV, were extracted from DFT calculations of the electronic spectrum of RuO_2 in Ref. [11]. Note that $J_A \neq J_B$ is a direct consequence of spin splitting of the electronic spectrum of altermagnets (for more details, see the SM [54]).

The LSWT spectrum of a noninteracting magnon in antiferromagnets is routinely derived [14,16] from a HP-transformed [13] effective spin Hamiltonian [Eq. (3)] in terms of bosonic operators (below, we assume spin value $S = 1/2$)

$$\hat{S}^z_{i,A} = \tfrac{1}{2} - \hat{a}^\dagger_i \hat{a}_i, \quad \hat{S}^z_{i,B} = \hat{b}^\dagger_i \hat{b}_i - \tfrac{1}{2}, \tag{4a}$$

$$\hat{S}^-_{i,A} = \sqrt{1 - \hat{a}^\dagger_i \hat{a}_i}\,\hat{a}_i, \; \hat{S}^-_{i,B} = \hat{b}^\dagger_i \sqrt{1 - \hat{b}^\dagger_i \hat{b}_i}, \tag{4b}$$

$$\hat{S}^+_{i,A} = \hat{a}^\dagger_i \sqrt{1 - \hat{a}^\dagger_i \hat{a}_i}, \; \hat{S}^+_{i,B} = \sqrt{1 - \hat{b}^\dagger_i \hat{b}_i}\,\hat{b}_i, \tag{4c}$$

after such transformations are *linearized*—$\hat{S}^z_{i,A(B)} = \frac{1}{2} - \hat{a}^\dagger_i \hat{a}_i (-\frac{1}{2} + \hat{b}^\dagger_i \hat{b}_i)$, $\hat{S}^-_{i,A(B)} = \hat{a}_i (\hat{b}^\dagger_i)$, and $\hat{S}^+_{i,A(B)} = \hat{a}^\dagger_i (\hat{b}_i)$—and the resulting HP Hamiltonian is truncated [7,56] to retain only quadratic terms in bosonic operators. In other words, one performs expansion [15,32] in $1/S$, starting with the order $1/S^2$, and retains only terms up to the order $(1/S)^{-1} = S$. Here, $\hat{a}_i$ ($\hat{a}^\dagger_i$) and $\hat{b}_i$ ($\hat{b}^\dagger_i$) destroy (create) a boson at site i within sublattices A and B, respectively. Equation (4a) clarifies that the number of such bosonic excitations at site i, as described by operators $\hat{a}^\dagger_i \hat{a}_i$ and $\hat{b}^\dagger_i \hat{b}_i$, captures the deviation of the magnetic quantum number from its maximum value $S = 1/2$. The same strategy leading to a quadratic and therefore exactly diagonalizable Hamiltonian can be applied to altermagnets. For this purpose, akin to the case of antiferromagnets, one applies the textbook [14] Bogoliubov-Valatin transformation of $\hat{a}_i$ ($\hat{a}^\dagger_i$) and $\hat{b}_i$ ($\hat{b}^\dagger_i$) into $\hat{\alpha}_i$ ($\hat{\alpha}^\dagger_i$) and $\hat{\beta}_i$ ($\hat{\beta}^\dagger_i$). From the thus-produced Hamiltonian (displayed explicitly in the SM [54]), which is exactly diagonalized by the Bogoliubov-Valatin transformation, we read off the energy-momentum dispersion of its two

nondegenerate magnon bands:

$$\hbar\omega(\mathbf{q}) = \pm\frac{\hbar}{2}[\omega_A(\mathbf{q}) - \omega_B(\mathbf{q})] + \frac{\hbar}{2}\sqrt{\omega_{AB}^2(\mathbf{q}) - 4\gamma(\mathbf{q})}. \quad (5)$$

Here, $\gamma(\mathbf{q})$ is the usual function [14] encoding the crystalline lattice properties and its spatial dimensionality. The sharp bands of Eq. (5) are plotted as red and orange lines in Figs. 1(a) and 1(e) for the case of the four-leg cylinder lattice in Fig. 2, where $\gamma(q_x, q_y) = J(\cos q_x a + \cos q_y a)$. We also use $\omega_{AB}(q_x) = \omega_A(q_x) + \omega_B(q_x)$, $\omega_A(q_x, q_y) = J - J_A/2 - J_B/2 + [J_A \cos(q_x + q_y)a + J_B \cos(q_x - q_y)a]/2$, and $\omega_B(q_x, q_y) = J - J_A/2 - J3_B/2 + [J_B \cos(q_x + q_y)a + J_A \cos(q_x - q_y)a]/2$, and a is the lattice constant.

All possible magnon-magnon interactions are described by an infinite series [7,56] (or finite, when such an infinite series is properly resumed [7,57,58]) of higher-order terms on top of the lowest-order quadratic HP Hamiltonian. By using TDMPSs, all such terms are automatically taken into account. We perform TDMPS calculations via a particular TDVP algorithm [37,43,59] implemented in the ITENSOR package [60] on a four-leg cylinder with four sites in the transverse direction and $N = 80$ sites in the longitudinal direction. We follow the same scheme as Ref. [39] to obtain the numerically exact retarded GF,

$$G(x, t) = -i\hbar\langle\Psi_0|\hat{S}_x^z(t)\hat{S}_c^z(0)|\Psi_0\rangle, \quad (6)$$

and from it the spectral function via Eq. (2). Note that the way to obtain these two quantities was originally demonstrated via a tDMRG algorithm applied to quantum spin chains [39]. The ground state (GS) $|\Psi_0\rangle$ is found using up to 30 sweeps and a maximum bond dimension $\chi = 200$, which guarantees a maximum error of $O(10^{-10})$. Then a wave packet is created by applying $\hat{S}_c^z|\Psi_0\rangle$ [39], where $c = 40$ is the lattice site in the middle of the ladder. The magnon spectral function in Eq. (2) is then obtained as the Fourier transform of Eq. (6) to frequency and momentum, where a Gaussian window function for the Fourier transform in time is typically employed [39].

Classical ASD simulations were performed on the same four-leg cylinder (Fig. 2) using a classical version of the Hamiltonian in Eq. (3) in which vectors of fixed length $\mathbf{S}_i(t)$ replace spin operators $\hat{\mathbf{S}}_i$ and are evolved by the stochastic (including temperature [55]) LLG equation [10,55]. This makes it possible to compute the DSSF [9]:

$$\mathcal{S}^{\alpha\alpha}(\mathbf{q}, \omega) = \frac{1}{\sqrt{2\pi}N}\sum_{\mathbf{r}_i, \mathbf{r}_j} e^{i\mathbf{q}\cdot(\mathbf{r}_i - \mathbf{r}_j)}\int_{-\infty}^{\infty} dt\, e^{i\omega t} C^{\alpha\alpha}(\mathbf{r}_i - \mathbf{r}_j, t). \quad (7)$$

Here, $\alpha = x, y, z$; N is the number of atoms per cell, and $C^{\alpha\alpha}(\mathbf{r}_i - \mathbf{r}_j, t) = \overline{S_i^\alpha(t)S_j^\alpha(0)} - \overline{S_i^\alpha(t)}\ \overline{S_j^\alpha(0)}$ measures correlations between spins, with $\overline{\cdots}$ denoting the ensemble average. Ensemble averaging is performed over different time segments during which a system of coupled LLG equations is solved to obtain trajectories $\mathbf{S}_i(t)$. The DSSF is directly measurable in neutron scattering experiments on bulk materials, or it can be obtained from spin-polarized high-resolution electron energy loss spectroscopy measurements on thin films [9]. By plotting $\mathcal{S}^{\alpha\alpha}(\mathbf{q}, \omega)$ in reciprocal space and by identifying the energies where its peaks appear [9], we extract the energy-momentum dispersion of magnons [Figs. 1(d) and 1(h)], in complete analogy to how dispersion is extracted from experimental neutron scattering data.

Results and discussion. The sharp bands of noninteracting magnons within LSWT track broadened and shifted interacting magnon bands *only* at the Brillouin zone (BZ) center or edges in Fig. 1(a), while deviating in other parts of BZ where broadening due to magnon-magnon interactions concurrently increases. Comparing Figs. 1(a) and 1(e), where the latter employs identical values of two exchange interaction constants $J_A = J_B$ between NN spins within sublattices A and B of the altermagnet, clarifies how such a discrepancy arises from $J_A \neq J_B$. This finding adds yet another case to the catalog of effective spin Hamiltonians [15–17,32,34–36,45] that can cause failure of LSWT. Deeper insight into the microscopic origin of the discrepancy can be obtained by analyzing higher-order $n > 2$ terms $\hat{H}_{\mathrm{HP}}^{(n)}$ in the Taylor series expansion [7,32,56] of the HP-bosonized effective spin Hamiltonian [Eq. (3)], $\hat{H}_{\mathrm{HP}} = \hat{H}_{\mathrm{HP}}^{(2)} + \hat{H}_{\mathrm{HP}}^{(4)} + O(1/S)$. Here, the subscript n denotes the presence of the nth power in bosonic operators. Note that all orders $\hat{H}_{\mathrm{HP}}^{(n)}$ are captured by numerically (quasi)exact TDMPS calculations, but terms $n > 4$ are progressively smaller, so we focus on the $n = 4$ term. Since $\hat{H}_{\mathrm{HP}}^{(3)}$, as the first correction to $\hat{H}_{\mathrm{HP}}^{(2)}$ of LSWT, is *zero* (the same applies to all other terms of odd n in collinear antiferromagnets [32]), one would naively expect [32] that magnon-magnon interactions encoded by $\hat{H}_{\mathrm{HP}}^{(4)}$ provide only a small correction. However, examples of frustrated antiferromagnets exist [36] in which $\hat{H}_{\mathrm{HP}}^{(4)}$ can open a channel for a large decay rate of magnons. Since $J_A \neq J_B$ is also a source of frustration, we analyze in Figs. 1(b) and 1(f) whether the one-magnon spectrum of LSWT is energetically degenerate with a three-magnon continuum, in which case $\hat{H}_{\mathrm{HP}}^{(4)} = \sum_{q_1,q_2,q_3} V_{q_1,q_2,q_3}\hat{\alpha}_{q_1}^\dagger\hat{\alpha}_{q_2}^\dagger\hat{\alpha}_{q_3}^\dagger\hat{\beta}_{q_1+q_2+q_3} + (\hat{\alpha} \leftrightarrow \hat{\beta}) + \mathrm{H.c.}$ for the case of the altermagnet that is the focus of our study can become effective. Figure 1(b) shows that the upper LSWT band overlaps with the three-magnon continuum, meaning that $\hat{H}_{\mathrm{HP}}^{(4)}$ will open a channel for decay of LSWT magnons into three-magnon states. The broadening of lower bands in Figs. 1(a) and 1(e), despite the *lack of degeneracy* between it and the three-magnon continuum [Fig. 1(b)], is actually an artifact of the window function employed when Fourier transforming Eq. (6) into Eq. (2). On the other hand, the broadening of the upper bands in Figs. 1(a) and 1(e) is a genuine consequence of magnon-magnon interactions encoded by $H_{\mathrm{HP}}^{(4)}$. While this term also shifts the upper band away from the LSWT upper band in Fig. 1(a), the upper band in Fig. 1(e) is only broadened without being renormalized. Note also that the upper band in Fig. 1(a) being shifted downward is the consequence of stronger hybridization on low-dimensional lattices [61], while on the 3D lattice of RuO_2 we expect band renormalization effects to be smaller.

The success of the LLG equation in numerical modeling, via classical micromagnetics [62] or ASD [9,10,55,63], of local magnetization within ferromagnets has also motivated its application to antiferromagnets [64–66] and, very recently, to altermagnets [67]. In the case of magnon spectrum calculation, ASD provides a computationally inexpensive (when compared to TDMPSs) route that can easily include

finite-temperature effects via stochastic terms in the LLG equation [9,10]. Due to the nonlinearity of the LLG equation, magnon-magnon interactions are intrinsically taken into account. The ASD-computed magnon spectrum in Figs. 1(d) and 1(h) exhibits bands that are similar to LSWT bands but broadened even at $T = 1$ K and using very small Gilbert damping $\alpha = 10^{-4}$ (larger damping would trivially increase broadening). Thus, the observed broadening independently confirms the importance of magnon-magnon interactions for the effective spin Hamiltonian of RuO_2 in Eq. (3), which is not simply an artifact of the low-dimensional lattice required for TDMPS calculations. However, ASD-broadened bands do not trace TDMPS calculations [Fig. 1(a) vs 1(d)] as magnon-magnon interactions captured quantum mechanically shift TDMPS bands away from either LSWT or ASD bands, in addition to broadening them more than in ASD. This failure of ASD to capture the TDMPS-computed magnon spectrum is not surprising, as it is well-known that antiferromagnets harbor entanglement [68,69] in their GS (leading to $\langle\Psi_0|\hat{\mathbf{S}}_i|\Psi_0\rangle = 0$ in both antiferromagnets and altermagnets) and excited states. Any residual entanglement in quantum states of magnons will make their classical description via the LLG equation *inapplicable* [70]. While it is naively expected that a finite temperature and large number of spins will diminish the entanglement of a macroscopically large number of spins, precisely such entanglement was detected very recently in the GS of antiferromagnets via neutron scattering experiments [71] up to a surprisingly high temperature $T \lesssim 200$ K. Furthermore, when antiferromagnets are pushed out of equilibrium, even stronger entanglement is produced [70] and can remain nonzero [70] (especially for spin $S = 1/2$ and $S = 1$) despite interactions with a dissipative environment.

A litmus test for the importance of magnon-magnon interactions via Raman scattering experiments. Raman scattering (RS), based on inelastic scattering of light [72–76] in which the kinetic energy of an incident photon is increased (Stokes RS) or reduced (anti-Stokes RS), offers a unique probe of collective excitations in solids. For example, RS has been applied to both magnons and phonons, where one also has to differentiate [74,76] their respective signals. Although RS probing of magnons lacks the momentum dependence of neutron scattering [21,71], it provides *high energy* resolution. In particular, two-magnon RS spectra reflect [74,77] the one-magnon density of states (DOS), thereby offering the following experimental RS-based litmus test for the importance of magnon-magnon interactions: (i) use the one-magnon dispersion of LSWT in Ref. [11] to obtain a DOS with a rescaled (by a factor of 2) energy scale; (ii) then measure two-magnon RS spectra experimentally and plot them together with the DOS obtained in the previous step; (iii) any discrepancy between these two curves signals the importance of magnon-magnon interactions. Figure 5 in Ref. [8] gives an example of the implementation of this test, and our Fig. 1(c) shows a clear distinction between LSWT- and TDMPS-computed magnon DOSs.

Conclusions. Comparing *three distinct* calculations of the magnon spectrum of the RuO_2 altermagnet—a quantum one-body calculation via LSWT, a quantum many-body calculation via TDMPS, and classical many-body calculation via ASD—divulges the following: (1) TDMPS bands of *interacting* magnons are shifted and broadened with respect to standard LSWT sharp bands [11] of noninteracting magnons, which is the signature of the relevance of magnon-magnon interactions in which one-magnon states can decay into a three-magnon continuum. (2) The distinction between the DOSs corresponding to these two spectra can be used to confirm the importance of magnon-magnon interactions; e.g., the recently obtained [11] magnon spectrum of RuO_2 (on its 3D lattice) and the corresponding DOS will not be able to explain two-magnon Raman scattering spectra if such interactions are indeed important for RuO_2. (3) Classical ASD calculations of magnon spectra [9], which are much less computationally expensive and highly popular [64–66] even for antiferromagnets, cannot trace quantum many-body calculations. The reason is entanglement as highly nonclassical effect that antiferromagnets and altermagnets often harbor [68–71] (in contrast, the success of LLG equation based simulations of magnon spectra of ferromagnets [9,10] can be rigorously justified [70] by the dissipative environment being able to completely wipe out their entanglement).

Acknowledgments. This research was supported by the U.S. National Science Foundation (NSF) through the University of Delaware Materials Research Science and Engineering Center, Grant No. DMR-2011824. The supercomputing time was provided by DARWIN (Delaware Advanced Research Workforce and Innovation Network), which is supported by NSF Grant No. MRI-1919839. The paper originated from Research Projects Based Learning implemented within the graduate course "PHYS800: Advanced Graduate Seminar in Quantum Physics" [78] at the University of Delaware.

[1] E. Kaxiras and J. D. Joannopoulos, *Quantum Theory of Materials* (Cambridge University Press, Cambridge, 2019).

[2] S. Konschuh, M. Gmitra, and J. Fabian, Tight-binding theory of the spin-orbit coupling in graphene, Phys. Rev. B **82**, 245412 (2010).

[3] E. Kogan, V. U. Nazarov, V. M. Silkin, and M. Kaveh, Energy bands in graphene: Comparison between the tight-binding model and *ab initio* calculations, Phys. Rev. B **89**, 165430 (2014).

[4] K. Held, Electronic structure calculations using dynamical mean field theory, Adv. Phys. **56**, 829 (2007).

[5] M. D. Watson, S. Backes, A. A. Haghighirad, M. Hoesch, T. K. Kim, A. I. Coldea, and R. Valentí, Formation of Hubbard-like bands as a fingerprint of strong electron-electron interactions in FeSe, Phys. Rev. B **95**, 081106(R) (2017).

[6] F. Bloch, Zur theorie des ferromagnetismus, Z. Phys. **61**, 206 (1930).

[7] U. Bajpai, A. Suresh, and B. K. Nikolić, Quantum many-body states and Green's functions of nonequilibrium electron-magnon systems: Localized spin operators versus their mapping to Holstein-Primakoff bosons, Phys. Rev. B **104**, 184425 (2021).

[8] M. A. Prosnikov, One- and two-magnon excitations in the antiferromagnet $PbFeBO_4$, Phys. Rev. B **103**, 094443 (2021).

[9] C. Etz, L. Bergqvist, A. Bergman, A. Taroni, and O. Eriksson, Atomistic spin dynamics and surface magnons, J. Phys.: Condens. Matter **27**, 243202 (2015).

[10] B. Skubic, J. Hellsvik, L. Nordström, and O. Eriksson, A method for atomistic spin dynamics simulations: Implementation and examples, J. Phys.: Condens. Matter **20**, 315203 (2008).

[11] L. Šmejkal, A. Marmodoro, K.-H. Ahn, R. González-Hernández, I. Turek, S. Mankovsky, H. Ebert, S. W. D'Souza, O. Šipr, J. Sinova, and T. Jungwirth, Chiral magnons in altermagnetic RuO_2, Phys. Rev. Lett. **131**, 256703 (2023).

[12] A. Szilva, Y. Kvashnin, E. A. Stepanov, L. Nordström, O. Eriksson, A. I. Lichtenstein, and M. I. Katsnelson, Quantitative theory of magnetic interactions in solids, Rev. Mod. Phys. **95**, 035004 (2023).

[13] T. Holstein and H. Primakoff, Field dependence of the intrinsic domain magnetization of a ferromagnet, Phys. Rev. **58**, 1098 (1940).

[14] E. M. Chudnovsky and J. Tejada, *Lectures on Magnetism* (Rinton, Princeton, NJ, 2006).

[15] M. E. Zhitomirsky and A. L. Chernyshev, *Colloquium*: Spontaneous magnon decays, Rev. Mod. Phys. **85**, 219 (2013).

[16] M. Gohlke, A. Corticelli, R. Moessner, P. A. McClarty, and A. Mook, Spurious symmetry enhancement in linear spin wave theory and interaction-induced topology in magnons, Phys. Rev. Lett. **131**, 186702 (2023).

[17] J. Habel, A. Mook, J. Willsher, and J. Knolle, Breakdown of chiral edge modes in topological magnon insulators, Phys. Rev. B **109**, 024441 (2024).

[18] Y. Li and W. E. Bailey, Wave-number-dependent Gilbert damping in metallic ferromagnets, Phys. Rev. Lett. **116**, 117602 (2016).

[19] L. Chen, C. Mao, J.-H. Chung, M. B. Stone, A. I. Kolesnikov, X. Wang, N. Murai, B. Gao, O. Delaire, and P. Dai, Anisotropic magnon damping by zero-temperature quantum fluctuations in ferromagnetic $CrGeTe_3$, Nat. Commun. **13**, 4037 (2022).

[20] P. Dai, H. Y. Hwang, J. Zhang, J. A. Fernandez-Baca, S.-W. Cheong, C. Kloc, Y. Tomioka, and Y. Tokura, Magnon damping by magnon-phonon coupling in manganese perovskites, Phys. Rev. B **61**, 9553 (2000).

[21] S. P. Bayrakci, D. A. Tennant, P. Leininger, T. Keller, M. C. R. Gibson, S. D. Wilson, R. J. Birgeneau, and B. Keimer, Lifetimes of antiferromagnetic magnons in two and three dimensions: Experiment, theory, and numerics, Phys. Rev. Lett. **111**, 017204 (2013).

[22] A. Chumak, V. Vasyuchka, A. Serga, and B. Hillebrands, Magnon spintronics, Nat. Phys. **11**, 453 (2015).

[23] A. V. Chumak, P. Kabos, M. Wu, C. Abert, C. Adelmann, A. O. Adeyeye, J. Akerman, F. G. Aliev, A. Anane, A. Awad *et al.*, Advances in magnetics roadmap on spin-wave computing, IEEE Trans. Magn. **58**, 1 (2022).

[24] P. Buczek, A. Ernst, P. Bruno, and L. M. Sandratskii, Energies and lifetimes of magnons in complex ferromagnets: A first-principle study of Heusler alloys, Phys. Rev. Lett. **102**, 247206 (2009).

[25] N. Tancogne-Dejean, F. Eich, and A. Rubio, Time-dependent magnons from first principles, J. Chem. Theory Comput. **16**, 1007 (2020).

[26] E. M. Hankiewicz, G. Vignale, and Y. Tserkovnyak, Inhomogeneous Gilbert damping from impurities and electron-electron interactions, Phys. Rev. B **78**, 020404(R) (2008).

[27] Y. Tserkovnyak, E. M. Hankiewicz, and G. Vignale, Transverse spin diffusion in ferromagnets, Phys. Rev. B **79**, 094415 (2009).

[28] C. A. Gallegos and A. L. Chernyshev, Magnon interactions in the quantum paramagnetic phase of $CoNb_2O_6$, Phys. Rev. B **109**, 014424 (2024).

[29] I. Bertelli, B. G. Simon, T. Yu, J. Aarts, G. E. W. Bauer, Y. M. Blanter, and T. van der Sar, Imaging spin-wave damping underneath metals using electron spins in diamond, Adv. Quantum Technol. **4**, 2100094 (2021).

[30] F. Reyes-Osorio and B. K. Nikolić, Nonlocal damping of spin waves in a magnetic insulator induced by normal, heavy, or altermagnetic metallic overlayer: A Schwinger-Keldysh field theory approach, Phys. Rev. B **110**, 214432 (2024).

[31] P. M. Bonetti and W. Metzner, Spin stiffness, spectral weight, and Landau damping of magnons in metallic spiral magnets, Phys. Rev. B **105**, 134426 (2022).

[32] A. L. Chernyshev and M. E. Zhitomirsky, Spin waves in a triangular lattice antiferromagnet: Decays, spectrum renormalization, and singularities, Phys. Rev. B **79**, 144416 (2009).

[33] A. B. Harris, D. Kumar, B. I. Halperin, and P. C. Hohenberg, Dynamics of an antiferromagnet at low temperatures: Spin-wave damping and hydrodynamics, Phys. Rev. B **3**, 961 (1971).

[34] K. Sourounis and A. Manchon, Impact of magnon interactions on transport in honeycomb antiferromagnets, Phys. Rev. B **110**, 054429 (2024).

[35] R. L. Smit, S. Keupert, O. Tsyplyatyev, P. A. Maksimov, A. L. Chernyshev, and P. Kopietz, Magnon damping in the zigzag phase of the Kitaev-Heisenberg-Γ model on a honeycomb lattice, Phys. Rev. B **101**, 054424 (2020).

[36] S. M. Winter, K. Riedl, P. A. Maksimov, A. L. Chernyshev, A. Honecker, and R. Valentí, Breakdown of magnons in a strongly spin-orbital coupled magnet, Nat. Commun. **8**, 1152 (2017).

[37] S. Paeckel, T. Köhler, A. Swoboda, S. Manmana, U. Schollwöck, and C. Hubig, Time-evolution methods for matrix-product states, Ann. Phys. (NY) **411**, 167998 (2019).

[38] Note that a comparison of the performance of the tDMRG and TDVP methods for different quantum spin Hamiltonians can be found in Ref. [44].

[39] S. R. White and A. E. Feiguin, Real-time evolution using the density matrix renormalization group, Phys. Rev. Lett. **93**, 076401 (2004).

[40] A. J. Daley, C. Kollath, U. Schollwöck, and G. Vidal, Time-dependent density-matrix renormalization-group using adaptive effective Hilbert spaces, J. Stat. Mech. (2004) P04005.

[41] P. Schmitteckert, Nonequilibrium electron transport using the density matrix renormalization group method, Phys. Rev. B **70**, 121302(R) (2004).

[42] A. E. Feiguin, The density matrix renormalization group and its time-dependent variants, AIP Conf. Proc. **1419**, 5 (2011).

[43] J. Haegeman, C. Lubich, I. Oseledets, B. Vandereycken, and F. Verstraete, Unifying time evolution and optimization with matrix product states, Phys. Rev. B **94**, 165116 (2016).

[44] T. Chanda, P. Sierant, and J. Zakrzewski, Time dynamics with matrix product states: Many-body localization transition of large systems revisited, Phys. Rev. B **101**, 035148 (2020).

[45] M. Mourigal, W. T. Fuhrman, A. L. Chernyshev, and M. E. Zhitomirsky, Dynamical structure factor of the triangular-lattice antiferromagnet, Phys. Rev. B **88**, 094407 (2013).

[46] Note that recent experimental [79] and theoretical [80] scrutiny found RuO_2 to be actually nonmagnetic in bulk form, but it remains an altermagnetic metal in the few-atomic-layer form [81]. Thus, these developments do not affect our study focused on just a single layer in Fig. 2, as well as on the general procedure for handling magnon-magnon interactions which can be applied to analyze a thereby induced modification of chiral magnon bands of other experimentally confirmed [82] altermagnetic materials.

[47] L. Šmejkal, J. Sinova, and T. Jungwirth, Emerging research landscape of altermagnetism, Phys. Rev. X **12**, 040501 (2022).

[48] L. Šmejkal, J. Sinova, and T. Jungwirth, Beyond conventional ferromagnetism and antiferromagnetism: A phase with nonrelativistic spin and crystal rotation symmetry, Phys. Rev. X **12**, 031042 (2022).

[49] S. Hayami, Y. Yanagi, and H. Kusunose, Momentum-dependent spin splitting by collinear antiferromagnetic ordering, J. Phys. Soc. Jpn. **88**, 023702 (2019).

[50] L.-D. Yuan, Z. Wang, J.-W. Luo, E. I. Rashba, and A. Zunger, Giant momentum-dependent spin splitting in centrosymmetric low-z antiferromagnets, Phys. Rev. B **102**, 014422 (2020).

[51] L. Šmejkal, R. González-Hernández, T. Jungwirth, and J. Sinova, Crystal time-reversal symmetry breaking and spontaneous Hall effect in collinear antiferromagnets, Sci. Adv. **6**, eaaz8809 (2020).

[52] I. I. Mazin, K. Koepernik, M. D. Johannes, R. González-Hernández, and L. Šmejkal, Prediction of unconventional magnetism in doped $FeSb_2$, Proc. Natl. Acad. Sci. USA **118**, e2108924118 (2021).

[53] A. T. Costa, J. C. G. Henriques, and J. Fernández-Rossier, Giant spatial anisotropy of magnon lifetime in altermagnets, arXiv:2405.12896.

[54] See Supplemental Material at http://link.aps.org/supplemental/10.1103/PhysRevB.111.L020407 for an additional figure showing how our LSWT exactly reproduces the "sharp bands" from Ref. [11] for RuO_2 on its 3D lattice, characterization of the GS of the altermagnetic four-leg cylinder in Fig. 2, further details of numerical procedures for obtaining the spectral function via TDMPS, quantification of spontaneous magnon decay rates, and the role of magnetic anisotropy, which also includes Refs. [83–89].

[55] R. Evans, W. Fan, P. Chureemart, T. Ostler, M. O. Ellis, and R. Chantrell, Atomistic spin model simulations of magnetic nanomaterials, J. Phys.: Condens. Matter **26**, 103202 (2014).

[56] S. Zheng, Z. Wang, Y. Wang, F. Sun, Q. He, P. Yan, and H. Yuan, Tutorial: Nonlinear magnonics, J. Appl. Phys. **134**, 151101 (2023).

[57] M. Vogl, P. Laurell, H. Zhang, S. Okamoto, and G. A. Fiete, Resummation of the Holstein-Primakoff expansion and differential equation approach to operator square roots, Phys. Rev. Res. **2**, 043243 (2020).

[58] J. König and A. Hucht, Newton series expansion of bosonic operator functions, SciPost Phys. **10**, 007 (2021).

[59] M. Yang and S. R. White, Time-dependent variational principle with ancillary Krylov subspace, Phys. Rev. B **102**, 094315 (2020).

[60] M. Fishman, S. R. White, and E. M. Stoudenmire, The ITensor software library for tensor network calculations, SciPost Phys. Codebases 4 (2022).

[61] R. Verresen, R. Moessner, and F. Pollmann, Avoided quasiparticle decay from strong quantum interactions, Nat. Phys. **15**, 750 (2019).

[62] D. V. Berkov and J. Miltat, Spin-torque driven magnetization dynamics: Micromagnetic modeling, J. Magn. Magn. Mater. **320**, 1238 (2008).

[63] UPPASD, https://github.com/UppASD/UppASD.

[64] R. Cheng, J. Xiao, Q. Niu, and A. Brataas, Spin pumping and spin-transfer torques in antiferromagnets, Phys. Rev. Lett. **113**, 057601 (2014).

[65] P. Li, J. Chen, R. Du, and X.-P. Wang, Numerical methods for antiferromagnets, IEEE Trans. Magn. **56**, 1 (2020).

[66] L. Moreels, I. Lateur, D. De Gusem, J. Mulkers, J. Maes, M. V. Milošević, J. Leliaert, and B. Van Waeyenberge, mumax+: extensible GPU-accelerated micromagnetics and beyond, arXiv:2411.18194.

[67] M. Weißenhofer and A. Marmodoro, Atomistic spin dynamics simulations of magnonic spin Seebeck and spin Nernst effects in altermagnets, Phys. Rev. B **110**, 094427 (2024).

[68] H. F. Song, N. Laflorencie, S. Rachel, and K. Le Hur, Entanglement entropy of the two-dimensional Heisenberg antiferromagnet, Phys. Rev. B **83**, 224410 (2011).

[69] A. Kamra, W. Belzig, and A. Brataas, Magnon-squeezing as a niche of quantum magnonics, Appl. Phys. Lett. **117**, 090501 (2020).

[70] F. Garcia-Gaitan and B. K. Nikolić, Fate of entanglement in magnetism under Lindbladian or non-Markovian dynamics and conditions for their transition to Landau-Lifshitz-Gilbert classical dynamics, Phys. Rev. B **109**, L180408 (2024).

[71] A. Scheie, P. Laurell, A. M. Samarakoon, B. Lake, S. E. Nagler, G. E. Granroth, S. Okamoto, G. Alvarez, and D. A. Tennant, Witnessing entanglement in quantum magnets using neutron scattering, Phys. Rev. B **103**, 224434 (2021).

[72] T. P. Devereaux and R. Hackl, Inelastic light scattering from correlated electrons, Rev. Mod. Phys. **79**, 175 (2007).

[73] P. Lemmens, G. Güntherodt, and C. Gros, Magnetic light scattering in low-dimensional quantum spin systems, Phys. Rep. **375**, 1 (2003).

[74] P. A. Fleury and R. Loudon, Scattering of light by one- and two-magnon excitations, Phys. Rev. **166**, 514 (1968).

[75] M. Cottam, Theory of two-magnon Raman scattering in antiferromagnets at finite temperatures, J. Phys. C **5**, 1461 (1972).

[76] M. T. Hutchings, M. F. Thorpe, R. J. Birgeneau, P. A. Fleury, and H. J. Guggenheim, Neutron and optical investigation of magnons and magnon-magnon interaction effects in NiF_2, Phys. Rev. B **2**, 1362 (1970).

[77] R. W. Davies, S. R. Chinn, and H. J. Zeiger, Spin-wave approach to two-magnon Raman scattering in a simple antiferromagnet, Phys. Rev. B **4**, 992 (1971).

[78] https://wiki.physics.udel.edu/phys800.

[79] M. Hiraishi, H. Okabe, A. Koda, R. Kadono, T. Muroi, D. Hirai, and Z. Hiroi, Nonmagnetic ground state in RuO_2 revealed by muon spin rotation, Phys. Rev. Lett. **132**, 166702 (2024).

[80] A. Smolyanyuk, I. I. Mazin, L. Garcia-Gassull, and R. Valentí, Fragility of the magnetic order in the prototypical altermagnet RuO_2, Phys. Rev. B **109**, 134424 (2024).

[81] S. G. Jeong, I. H. Choi, S. Nair, L. Buiarelli, B. Pourbahari, J. Y. Oh, N. Bassim, A. Seo, W. S. Choi, R. M. Fernandes, T. Birol, L. Zhao, J. S. Lee, and B. Jalan, Altermagnetic polar metallic phase in ultra-thin epitaxially-strained RuO_2 films, arXiv:2405.05838.

[82] Z. Liu, M. Ozeki, S. Asai, S. Itoh, and T. Masuda, Chiral split magnon in altermagnetic MnTe, Phys. Rev. Lett. **133**, 156702 (2024).

[83] T. Berlijn, P. C. Snijders, O. Delaire, H.-D. Zhou, T. A. Maier, H.-B. Cao, S.-X. Chi, M. Matsuda, Y. Wang, M. R. Koehler, P. R. C. Kent, and H. H. Weitering, Itinerant antiferromagnetism in RuO_2, Phys. Rev. Lett. **118**, 077201 (2017).

[84] S. Sugiura and A. Shimizu, Thermal pure quantum states at finite temperature, Phys. Rev. Lett. **108**, 240401 (2012).

[85] S. Sugiura and A. Shimizu, Canonical thermal pure quantum state, Phys. Rev. Lett. **111**, 010401 (2013).

[86] Y. Gao, J. Wang, Q. Li, Q.-B. Yan, T. Shi, and W. Li, Magnon damping minimum and logarithmic scaling in a Kondo-Heisenberg model, arXiv:2401.00758.

[87] S. Yan, D. A. Huse, and S. R. White, Spin-liquid ground state of the S = 1/2 kagome Heisenberg antiferromagnet, Science **332**, 1173 (2011).

[88] W. H. Press, S. A. Teukolsky, W. T. Vetterling, and B. P. Flannery, *Numerical Recipes: The Art of Scientific Computing* (Cambridge University Press, Cambridge, 2007).

[89] F. J. dos Santos, M. dos Santos Dias, F. S. M. Guimarães, J. Bouaziz, and S. Lounis, Spin-resolved inelastic electron scattering by spin waves in noncollinear magnets, Phys. Rev. B **97**, 024431 (2018).

Supplemental Material for "Magnon spectrum of altermagnets beyond linear spin wave theory: Magnon-magnon interactions via time-dependent matrix product states vs. atomistic spin dynamics"

Federico Garcia-Gaitan, Ali Kefayati, John Q. Xiao, and Branislav K. Nikolić*
Department of Physics and Astronomy, University of Delaware, Newark, DE 19716, USA

This Supplemental Material provides *five* additional Figs. S1-Fig. S5 and further details of: our linear spin wave theory (LSWT), as well as how it reproduces "sharp bands" of RuO_2 on its 3D lattice from Ref. [1]; characterization of the ground state (GS) of altermagnetic 4-leg cylinder in Fig. 1 in the main text; further details of numerical procedures for obtaining spectral function via time-dependent matrix product states (TDMPS) calculations; and the role of magnetic anisotropy.

I. LINEAR SPIN WAVE THEORY FOR ALTERMAGNETIC EFFECTIVE SPIN HAMILTONIAN

We considered the effective spin Hamiltonian of RuO_2, as derived in Ref. [1] from first principles, where localized spins on the sites i of a three-dimensional (3D) lattice are described by spin-1/2 operators $\hat{\mathbf{S}}_i$

$$\hat{H} = J\sum_{\langle ij\rangle}\hat{\mathbf{S}}_i\cdot\hat{\mathbf{S}}_j + J_1\sum_{\langle\langle ij\rangle\rangle}\hat{\mathbf{S}}_i\cdot\hat{\mathbf{S}}_j + \sum_{\langle\langle\langle ij\rangle\rangle\rangle}J_{ij}\hat{\mathbf{S}}_i\cdot\hat{\mathbf{S}}_j, \tag{S1}$$

which is different from Hamiltonian in Eq. (3) of the main text by containing additional third term where spins interact with the next-next nearest neighbors (NN) Heisenberg exchange couplings J_{ij}. Note that J_{ij} takes only two values, $J_{ij} = J_2$ or $J_{ij} = J_3$, which are dependent on the relative orientation of the two localized spins. The Holstein-Primakoff (HP) transformation [2, 3], which maps spin operators to bosonic ones, requires to first determine the classical GS. This state can be found using the method of magnetic torques [4], and turns out to be the same [1, 5] as the GS of antiferromagnets (AFs). Therefore, HP transformations for altermagnet proceed in the same way as the textbook [6] ones for AFs

$$\hat{S}^z_{i,A} = \frac{1}{2} - \hat{a}^\dagger_i\hat{a}_i,\ \hat{S}^z_{i,B} = \hat{b}^\dagger_i\hat{b}_i - \frac{1}{2}, \tag{S2a}$$

$$\hat{S}^-_{i,A} = \sqrt{1-\hat{a}^\dagger_i\hat{a}_i}\hat{a}_i \simeq \sqrt{2S}\hat{a}_i,\ \hat{S}^-_{i,B} = \hat{b}^\dagger_i\sqrt{1-\hat{b}^\dagger_i\hat{b}_i} \simeq \hat{b}^\dagger_i\sqrt{2S}, \tag{S2b}$$

$$\hat{S}^+_{i,A} = \hat{a}^\dagger_i\sqrt{1-\hat{a}^\dagger_i\hat{a}_i} \simeq \hat{a}^\dagger_i\sqrt{2S},\ \hat{S}^+_{i,B} = \sqrt{1-\hat{b}^\dagger_i\hat{b}_i}\hat{b}_i \simeq \sqrt{2S}\hat{b}_i. \tag{S2c}$$

After linearization of HP transformation, as shown in Eqs. (S2b) and (S2c), and switching to momentum representation

$$\hat{a}_i = \frac{1}{\sqrt{N}}\sum_{\mathbf{q}} e^{i\mathbf{q}\cdot\mathbf{r}_i}\hat{a}_{\mathbf{q}}, \tag{S3a}$$

$$\hat{b}_i = \frac{1}{\sqrt{N}}\sum_{\mathbf{q}} e^{i\mathbf{q}\cdot\mathbf{r}_i}\hat{b}_{\mathbf{q}}, \tag{S3b}$$

Hamiltonian in Eq. (S1) is transformed into the LSWT Hamiltonian (linear in S):

$$\hat{H}^{(2)}_{\mathrm{HP}} = Sq\sum_{\mathbf{q}}\left(\hbar\omega_A(\mathbf{q})\hat{a}^\dagger_{\mathbf{q}}\hat{a}_{\mathbf{q}} + \hbar\omega_B(\mathbf{q})\hat{b}^\dagger_{-\mathbf{q}}\hat{b}_{-\mathbf{q}} + \gamma_{\mathbf{q}}\hat{a}_{\mathbf{q}}\hat{b}_{-\mathbf{q}} + \gamma^*_{\mathbf{q}}\hat{a}^\dagger_{\mathbf{q}}\hat{b}^\dagger_{-\mathbf{q}}\right). \tag{S4}$$

Here $\omega_{A(B)}(\mathbf{q}) = J - J_1 - J_2/2 - J_3/2 + J_1\gamma_1(\mathbf{q}) + J_{2(3)}\gamma_2(\mathbf{q}) + J_{3(2)}\gamma_3(\mathbf{q})$; and parameters

$$\gamma_{\mathbf{q}} = 1/z\sum_{\boldsymbol{\delta}} e^{-i\mathbf{q}\cdot\boldsymbol{\delta}},\ \gamma_1(\mathbf{q}) = 1/z\sum_{\boldsymbol{\delta}}\cos\mathbf{q}\cdot\boldsymbol{\delta},\ \gamma_2(\mathbf{q}) = 1/z\sum_{\boldsymbol{\delta'}}\cos\mathbf{q}\cdot\boldsymbol{\delta'},\ \gamma_3(\mathbf{q}) = 1/z\sum_{\boldsymbol{\delta''}}\cos\mathbf{q}\cdot\boldsymbol{\delta''}, \tag{S5}$$

* bnikolic@udel.edu

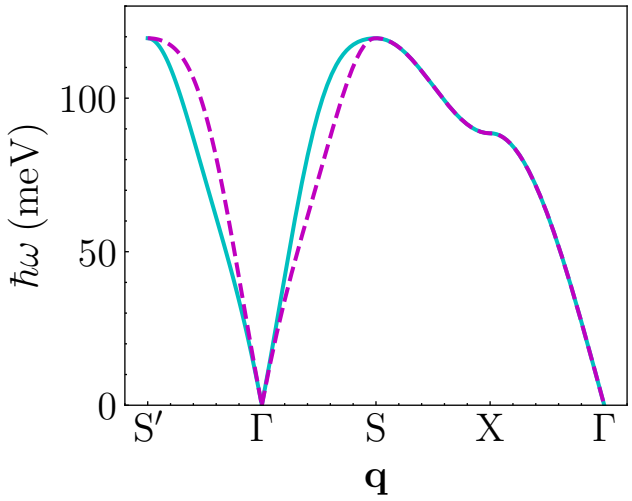

FIG. S1. Energy-momentum dispersion from Eq. (S8) produced by LSWT of section I reproduces magnon bands from Ref. [1] of RuO_2 on its 3D lattice.

encode geometrical properties of the lattice, where z is the coordination number and $\boldsymbol{\delta}$, $\boldsymbol{\delta'}$, $\boldsymbol{\delta''}$ are vectors pointing towards the NN or next-NN, respectively. The LSWT Hamiltonian [Eq. (S4)] is quadratic in HP bosonic operators and, therefore, easily diagonalizable by the textbook [6] Bogoliubov-Valantin transformation

$$\begin{pmatrix} \hat{a}_{\mathbf{q}} \\ \hat{b}^{\dagger}_{-\mathbf{q}} \end{pmatrix} = \begin{pmatrix} u_{\mathbf{q}} & v_{\mathbf{q}} \\ v_{\mathbf{q}} & u_{\mathbf{q}} \end{pmatrix} \begin{pmatrix} \hat{\alpha}_{\mathbf{q}} \\ \hat{\beta}^{\dagger}_{\mathbf{q}} \end{pmatrix}, \tag{S6}$$

leading to

$$\hat{H}^{(2)}_{\mathrm{HP}} = Sz \sum_{\mathbf{q}} \hbar\omega_{\alpha}(\mathbf{q}) \left(\hat{\alpha}^{\dagger}_{\mathbf{q}} \hat{\alpha}_{\mathbf{q}} + \frac{1}{2} \right) + \hbar\omega_{\beta}(\mathbf{q}) \left(\hat{\beta}^{\dagger}_{\mathbf{q}} \hat{\beta}_{\mathbf{q}} + \frac{1}{2} \right), \tag{S7}$$

from which we read the following energy-momentum disperions of two non-degenerate magnon bands

$$\hbar\omega(\mathbf{q}) = \pm \frac{\hbar}{2} \left[\omega_A(\mathbf{q}) - \omega_B(\mathbf{q}) \right] + \frac{\hbar}{2} \sqrt{\left[\omega_A(\mathbf{q}) + \omega_B(\mathbf{q}) \right]^2 - (2J\gamma_{\mathbf{q}})^2}. \tag{S8}$$

These two bands are plotted in Fig. S1, and they fully reproduce Fig. 3 of Ref. [1]. Note that the first term in Eq. (S8) is responsible for band splitting, and the two bands are compensated in the sense that the sign of the energy difference changes as we sweep $\mathbf{q}$ vector in the first Brillouin zone (BZ). In Eq. (S7) we make explicit the zero-point energy terms, $\hbar\omega_{\alpha(\beta)}(\mathbf{q})/2$, as second-quantized description of entangled GS of altermagnet or AF [7–9]. When we switch from 3D lattice to 4-leg cylinder [Fig. 1 of the main text] employed in TDMPS calculations of the main text, the dispersion in Eq. (S8) becomes Eq. (5) of the main text.

II. CONFIRMATION OF MAINTENANCE OF ALTERMAGNETIC PROPERTIES FOR SPIN HAMILTONIAN DEFINED ON 4-LEG CYLINDER

Since numerically (quasi)exact TDMPS calculations are restricted [10] to quasi-one-dimensional lattices, we put effective spin Hamiltonian [Eq. (S1)] of RuO_2 derived in Ref. [1] onto a square lattice of 80×4 sites. By connecting spins on sites 1 and 4 along the transverse direction via exchange couplings, we introduce a 4-leg cylinder employed in the main text. These types of cylindrical lattices have often been used in MPS and TDMPS calculations [11]. We find that 4 sites along the transverse direction are minimally required for hosting the symmetry group of both electron and spin subsystems within RuO_2 altermagnet. In particular, the 4-leg cylinder allows for AF ordering of localized spins, where the symmetry transformation between spins belonging to different sublattices is π rotation [Fig. 1(b) of the main text]. The symmetry transformation for electronic orbital degrees of freedom is $\pi/2$ rotation [Fig. 1(b) of the main text]. Note that the orbital symmetry is imposed by fixing the values of the Heisenberg exchange parameters.

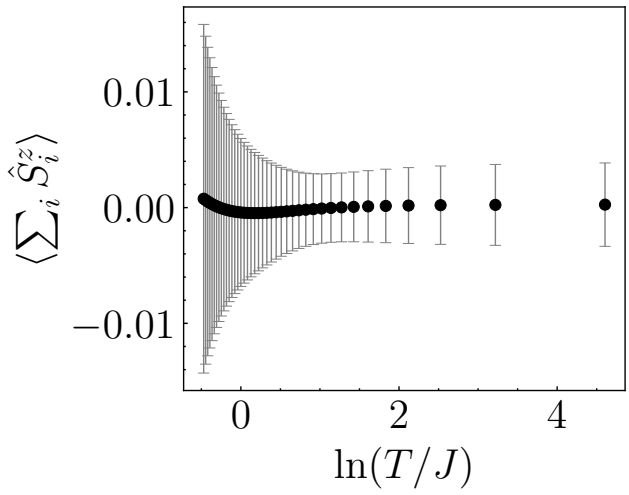

FIG. S2. Expectation value of total spin along the z-axis as a function of temperature computed for a 4×4 square lattice with periodic boundary conditions in both directions using the TPQS method [12, 13]. Error bars quantify statistical error when averaging over 100 different TPQS at a given temperature.

On the other hand, if Heisenberg exchange parameters are changed to deviate from each other too much, thereby causing strong frustration, the electronic energy spectrum will lose its altermagnetic properties.

We further demonstrate in Fig. S2 that altermagnetic spin Hamiltonian put onto 4-leg cylinder does not develop any nonzero magnetization at finite temperature. For this purpose, we add a small magnetic field at one site, $\hat{H}_B = B_z \hat{S}_1^z$, in order to break rotational symmetry. We compute quantum statistical average using the thermal pure quantum state (TPQS) methodology [12, 13] which bypasses computationally more expensive (as it requires full diagonalization of the Hamiltonian) evaluation of equilibrium density matrix.

Another defining property of altermagnets which must be maintained by our 4-leg cylinder model is their collinear antiferromagnetic ordering. We verified in two ways: (*i*) the minimum energy configuration of the classical version of Hamiltonian in Eq. (3) of the main text was found to always be the Néel state; (*ii*) the static spin structure factor of the GS of quantum Hamiltonian has maximum at (π, π) [Fig. S3], which confirms AF ordering of localized quantum spins [5].

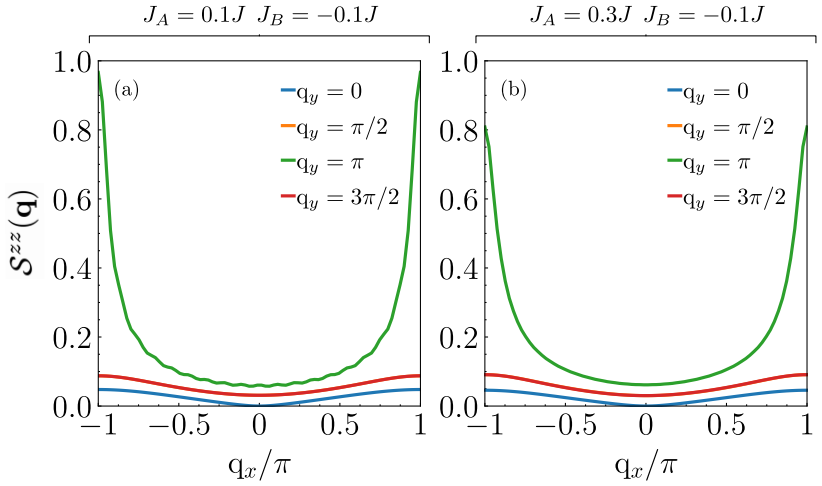

FIG. S3. TDMPS-computed static spin structure factor $\mathcal{S}^{zz}(q_x)$ of two different GSs of altermagnetic spin Hamiltonian in Eq. (3) of the main text put onto 4-leg cylinder. The two GSs are obtained by using two different sets [see top of panels (a) and (b)] of exchange couplings that are also employed in Fig. 2 of the main text.

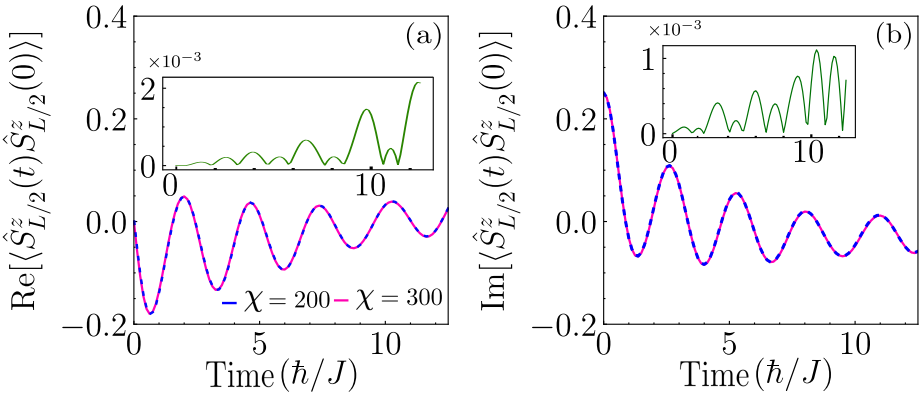

FIG. S4. Convergence check of TDVP calculations [14] using example of two-time spin-spin correlation functions for altermagnetic effective spin Hamiltonian [Eq. (3) in the main text] on 4-leg cylinder [Fig. 1 in the main text]: (a) real-part of such correlator; (b) imaginary part of such correlator. Two bond dimensions [10, 14] in TDMPS calculations, $\chi = 200$ and $\chi = 300$, are considered and the absolute difference between their respective (blue and red) curves is shown in the inset (green curve) of each panel.

III. TECHNICAL DETAILS OF TDMPS CALCULATIONS

Our TDMPS calculations proceed via time-dependent variational principle (TDVP) version of it, as implemented in `ITensor` package [14]. For computationally efficient usage of TDVP, we map 4-leg cylinder of Sec. II to one-dimensional chain whose localized spins have Hilbert space of dimension 2^4 instead of 2 for $S = 1/2$. Using this procedure, we obtain retarded Green's function (GF) in Eq. (6) of the main text. Note that the same Eq. (6) was originally evaluated for different spin quantum system as an example of early developments of time-dependent density matrix renormalization group [15]. We compute time evolution via TDVP using the same maximum bond dimension $\chi = 200$ as employed to find the GS, and with time step $\delta t = 0.125\hbar/J$ and total propagation time of $20\hbar/J$ [which guarantees a maximum error of $\mathcal{O}(10^{-6})$]. Note that the real time evolution is limited by finite length of the system. Indeed, the correlation will spread with a characteristic light cone dispersion and, thus, once it reaches the edges of the system it could produce unphysical results. As a convergence test, we varied the maximum bond dimension between $\chi = 200$ and $\chi = 300$ and then compared the real-time spin-spin correlation function for different χ parameters, as shown in Fig. S4. Since we find only a minuscule difference, Fig. S4 demonstrates that our results in the main text are already properly converged.

As discussed in the main text, converting retarded GF, as a function of real space and time, into a spectral function $A(\mathbf{q}, \omega)$, as a function of wavevector and frequency, requires a Fourier transform between the two sets of variables. The transform also involves Gaussian window function [16] which can introduce artifactual broadening of magnon bands. To minimize such broadening, one often employs linear predictor [16] methodology which allows one to forecast time series and, thereby, extend the simulation time. In turn, the longer simulation time makes it possible to reduce the artifactual broadening.

IV. MAGNETIC ANISOTROPY EFFECT ON MAGNON DECAY RATE

An effective way to reduce magnon decay is offered by the control via increasing magnetic anisotropy. This reduces quantum fluctuations and stabilizes the classical Néel order, i.e., increased anisotropy favors Ising-like exchange interactions terms which then reduces the effect of magnon-magnon interactions. As an example of such an effect, we consider standard [6] XXZ Heisenberg quantum AF ladder (i.e., 80×2 lattice) and compute its magnon spectral function via TDVP. Figure S5(a) shows that "sharp magnon" bands are blurred in the middle of the BZ because of the importance of magnon-magnon interactions for the case of XXX isotropic Heisenberg quantum AF. On the other hand, increasing anisotropy along the z-axis (which is orthogonal to the ladder), and thereby switching to XXZ model in Fig. S5(c), makes magnon band well-defined across the whole BZ. Note that bright yellow traces in Fig. S5(c) are the counterpart when plotting spectral function of the "sharp bands" of LSWT, while their broadening due to magnon-magnon interactions is depicted by blue traces surrounding them [17]. Note also that the finite size of the lattice induces a gap of the order of J_z, which facilitates convergence of TDMPS calculations.

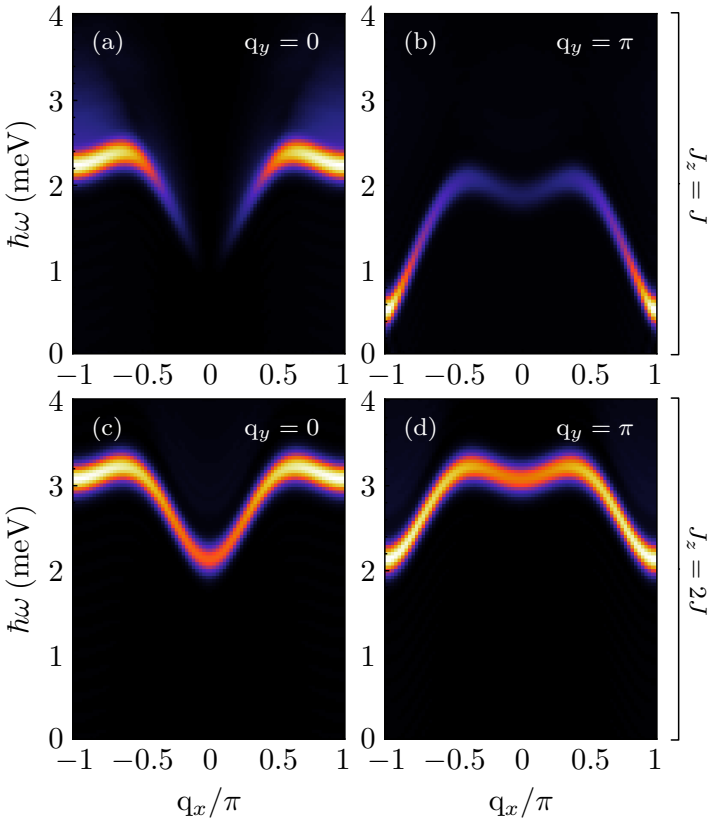

FIG. S5. Magnon energy-momentum dispersion from TDMPS-computed spectral function $A(\mathbf{q}, \omega)$ [Eq. (2) in the main text] for: (a),(b) isotropic XXX; and (c),(d) anisotropic XXZ Heisenberg quantum AF on a ladder. The magnetic anisotropy along the z-axis, orthogonal to the ladder, is introduced by using $J_x = J_y = J$ and $J_z = 2J$ in the XXZ case, while $J_x = J_y = J_z = J$ in the XXX case.

[1] L. Šmejkal, A. Marmodoro, K.-H. Ahn, R. González-Hernández, I. Turek, S. Mankovsky, H. Ebert, S. W. D'Souza, O. Šipr, J. Sinova, and T. Jungwirth, Chiral magnons in altermagnetic RuO_2, Phys. Rev. Lett. **131**, 256703 (2023).

[2] T. Holstein and H. Primakoff, Field dependence of the intrinsic domain magnetization of a ferromagnet, Phys. Rev. **58**, 1098 (1940).

[3] U. Bajpai, A. Suresh, and B. K. Nikolić, Quantum many-body states and Green's functions of nonequilibrium electron-magnon systems: Localized spin operators versus their mapping to Holstein-Primakoff bosons, Phys. Rev. B **104**, 184425 (2021).

[4] F. J. dos Santos, M. dos Santos Dias, F. S. M. Guimarães, J. Bouaziz, and S. Lounis, Spin-resolved inelastic electron scattering by spin waves in noncollinear magnets, Phys. Rev. B **97**, 024431 (2018).

[5] T. Berlijn, P. C. Snijders, O. Delaire, H.-D. Zhou, T. A. Maier, H.-B. Cao, S.-X. Chi, M. Matsuda, Y. Wang, M. R. Koehler, P. R. C. Kent, and H. H. Weitering, Itinerant antiferromagnetism in RuO_2, Phys. Rev. Lett. **118**, 077201 (2017).

[6] E. M. Chudnovsky and J. Tejada, *Lectures on Magnetism* (Rinton Press, Princeton, 2006).

[7] H. F. Song, N. Laflorencie, S. Rachel, and K. Le Hur, Entanglement entropy of the two-dimensional Heisenberg antiferromagnet, Phys. Rev. B **83**, 224410 (2011).

[8] A. Kamra, W. Belzig, and A. Brataas, Magnon-squeezing as a niche of quantum magnonics, Appl. Phys. Lett. **117**, 090501 (2020).

[9] F. Garcia-Gaitan and B. K. Nikolić, Fate of entanglement in magnetism under Lindbladian or non-Markovian dynamics and conditions for their transition to Landau-Lifshitz-Gilbert classical dynamics, Phys. Rev. B **109**, L180408 (2024).

[10] S. Paeckel, T. Köhler, A. Swoboda, S. Manmana, U. Schollwöck, and C. Hubig, Time-evolution methods for matrix-product states, Ann. Phys. **411**, 167998 (2019).

[11] S. Yan, D. A. Huse, and S. R. White, Spin-liquid ground state of the S = 1/2 Kagome Heisenberg antiferromagnet, Science **332**, 1173 (2011).

[12] S. Sugiura and A. Shimizu, Thermal pure quantum states at finite temperature, Phys. Rev. Lett. **108**, 240401 (2012).

[13] S. Sugiura and A. Shimizu, Canonical thermal pure quantum state, Phys. Rev. Lett. **111**, 010401 (2013).
[14] M. Fishman, S. R. White, and E. M. Stoudenmire, The ITensor software library for tensor network calculations, SciPost Phys. Codebases , 4 (2022).
[15] S. R. White and A. E. Feiguin, Real-time evolution using the density matrix renormalization group, Phys. Rev. Lett. **93**, 076401 (2004).
[16] W. H. Press, S. A. Teukolsky, W. T. Vetterling, and B. P. Flannery, *Numerical Recipes: The Art of Scientific Computing* (Cambridge University Press, Cambridge, 2007).
[17] S. M. Winter, K. Riedl, P. A. Maksimov, A. L. Chernyshev, A. Honecker, and R. Valentí, Breakdown of magnons in a strongly spin-orbital coupled magnet, Nat. Comm. **8**, 1152 (2017).